Reactive VLS and the Reversible Switching between VS and VLS Growth Modes for ZnO Nanowire Growth

Niranjan S. Ramgir,*,† Kittitat Subannajui,† Yang Yang,†,‡ Raphael Grimm,† Rebecca Michiels,† and Margit Zacharias*,†

Nanotechnology Group, Institute of Microsystems Engineering-IMTEK, Georges-Kohler Allee 103, University of Freiburg, Freiburg, 79110, Germany, and Max Planck Institute of Microstructure Physics, Weinberg 2, 06120 Halle, Germany

Received: September 30, 2009; Revised Manuscript Received: March 18, 2010

The controlled reversible switching between vapor−solid (VS) and vapor−liquid−solid (VLS) growth of ZnO nanowires (NWs) mediated by organic solvents, namely, ionic liquids (ILs), is demonstrated. Suppression or enhancement of the VLS mechanism is achieved by the control of Zn oxidation and ZnO reduction by the abundant IL pyrolyzates working as an additional carbon source. A new model called *reactive VLS mode* based on the Zn−Au alloy and the immediate oxidation of the out-sourced Zn is suggested. Cleaning the tube with concentrated HCl completely reverses the growth from the VLS back to the VS mechanism. The VLS NWs show a strong band-gap luminescence, whereas in the case of VS NWs, the defect luminescence is enhanced. Our results clarify, for the first time, the reason for the different roles of Au, that is, acting *as surface defects or as a catalyst in VS and VLS growth modes*, respectively. In addition, our results demonstrate the possibility of changing not only the growth mode and extending the growth region but also the NWs' crystal quality using ILs as an additional carbon source.

Introduction

Among the various nanostructures based on semiconducting oxides, ZnO has been studied because of its direct wide band gap (3.37 eV), large exciton binding energy (60 meV), and potential use in a number of applications, such as field effect transistors (FETs),[1,2] bio/chemical sensors,[3] light-emitting devices,[4] and solar cells.[5] However, using ZnO NWs in various kinds of devices requires a careful control of their structural and physical properties, which can be achieved by controlling the respective growth process.[6,7] Vapor phase deposition is the most widely studied growth process for ZnO NWs and results in a large variety of nanostructures. The unique wurtzite structure of ZnO with its noncentral symmetry and polar surfaces is represented by alternating planes composed of tetrahedrally coordinated O^{2-} and Zn^{2+} ions stacked along the *c* axis. The oppositely charged ions produce positively charged (0001) Zn and negatively charged $(000\bar{1})$ O polar surfaces resulting in divergence in surface energy. In addition, a normal dipole moment and spontaneous polarization along the *c* axis is observed. In particular, ZnO has three directions of fast growth: one polar (*c*-plane) (0001) (±[0001]) and two nonpolar, namely, $(01\bar{1}0)$ (±$[01\bar{1}0]$, ± $[10\bar{1}0]$, ± $[1\bar{1}00]$) and $(2\bar{1}\bar{1}0)$ (±$[2\bar{1}\bar{1}0]$, ± $[\bar{1}2\bar{1}0]$, ± $[\bar{1}\bar{1}20]$). Accordingly, various exotic nanostructures, such as nanorings,[8] nanonails,[9] and nanohelices,[10] are found as a result of the minimization of the total energy forced by spontaneous polarization, surface area optimization, and elastic deformation.

The use of metal nanoparticles as catalysts is specific for the vapor−liquid−solid (VLS) as well as the vapor−solid (VS) processes, where the catalyst initiates and guides the growth. An epitaxial relationship between the substrate and the NWs is needed to grow NWs in a patterned and aligned arrangement based on either the VLS or the VS mode. In principal, the VLS growth process is characterized by the presence of a metal particle at the NW tip[11] and offers the possibility for diameter and arrangement control via the patterned arrays of catalyst. A carrier gas (usually Ar) transports the vaporized source material to the catalyst droplet (Au, Ag, and Ni).[12] The vapor source material adsorbs and diffuses into the metal catalyst, forming a *liquid* alloy. With time, the concentration will exceed the solubility and precipitation in the form of NWs is observed. This supersaturation and precipitation process continues until the source material is exhausted or the growth conditions are no longer preserved (lowering of pressure or temperature).

On the other hand, the VS process involves the transport of the vapor species from the source to the substrate and their subsequent (enhanced) condensation on the still solid (metal) catalyst.[13−15] Surface defects, dislocations, or metal patterns on the substrate can provide energetically favored nucleation sites for the incoming vapor. At these sites, Zn solidifies quickly to ZnO by oxidation when oxygen is either intentional or unintentional in the reaction chamber, especially at places with inhomogeneties or defects, and creates ZnO wires or vortex-like nanostructures.[16] VS NWs are observed to grow slower (10−100 times) than VLS NWs because of the lower diffusivity, the contributions of desorption, and the weaker surface reactivity in the solid phases.

Up to now NWs are reported grown by *either VS or VLS*, but a systematic transition of the growth process by means of controlling specific process parameters has not been demonstrated so far. Also, the reason for the different roles of the Au, that is, as a catalyst for VLS or as a surface defect for VS growth, is not completely understood so far, especially in the case of ZnO. Besides, a complete understanding of the growth process, which enables a control of crystal quality (defects,

* To whom correspondence should be addressed. E-mail: niranjanpr@indiatimes.com; zacharias@imtek.uni-freiburg.de. Tel: + 0049 761 203 7214. Fax: + 0049 761 203 7262.
† Institute of Microsystems Engineering-IMTEK.
‡ Max Planck Institute of Microstructure Physics.

10.1021/jp909377b
Published on Web 05/20/2010

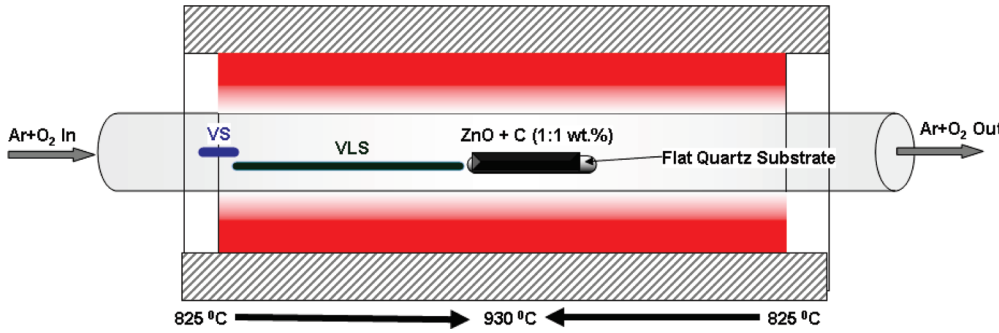

Figure 1. Schematic illustration of the growth setup exhibiting the drastic change in the region of NW growth after the use of the IL drop-cast on the Si substrate (VS/VLS).

charge carrier concentration) by tuning process parameters, is demanded for their direct integration into device application. In the present study, we report the controlled and reversible transition of the growth mode from VS to VLS by simply applying ionic liquids (ILs), namely, butyl methyl imadazolium tetrafluoroborate ($BMIm^+BF_4^-$) and butyl methyl imadazolium hexafluorophosphate ($BMIm^+PF_6^-$), as an additional carbon source. The presence of the additional carbon is responsible for the formation of a liquid Au−Zn alloy dot that is crucial for the VLS mechanism. The influence of the ionic liquid on the growth mode, NW diameter, crystal quality, orientation, and the observation of kink structures will be discussed in detail.

Experimental Section

Nanowire Growth. ZnO NWs were grown by surface-catalyzed vapor-phase deposition. GaN/sapphire substrates were first hydrophilized by treating the substrates in piranha solution (3:1 H_2SO_4/H_2O_2) at 80 °C for 20 min. Nanosphere lithography was used to realize a Au pattern on the substrates. In brief, a 20 nm Au film was evaporated through the nanosphere mask. The nanosphere mask was removed by dichloromethane, and the substrate was subjected to oxygen plasma cleaning. Annealing at 500 °C for 10 min in air was carried out to form circular Au dots. The size of the resulting Au dots was investigated by scanning electron microscopy and found to be in the range of up to 70 nm. For NW growth, the source powders (ZnO, Aldrich 99.999%; graphite, Alfa-Aesar ~200 mesh) were mixed at a weight ratio of 1:1. The source powder (~0.450 g) and the substrates were placed inside the horizontal 1 in. diameter quartz tube furnace as shown in Figure 1. The gas is confined inside the tube, and the reaction occurs homogeneously. The vacuum seals were firmly tightened to prevent any unwanted O_2 leaking in from ambient. A leak test has been performed by observing the change of static pressure (200 mbar) inside the closed tube, monitoring the leakage rate, which was negligible. Argon ($Ar_{(g)}$, flow rate of 7 sccm) with oxygen (0.001 sccm) is used as the carrier gas flowing from left to right in the furnace (Figure 1). The growth pressure is kept constant at 200 mbar. The NWs were grown for 10−35 min (heating duration) at substrate temperatures between 875 and 930 °C using the temperature gradient of the furnace. The IL (5 μL) was drop-cast onto a blank Si wafer and kept next to the substrates containing the patterned Au. After approximately three to five experiments with IL-treated pieces in the same tube, the growth mode changes and the wire growth zone drastically extends toward the center of the furnace, covering even the complete homogeneous temperature zone.

Nanowire Characterization. Structural details of the NWs, including surface morphologies, were examined using field emission scanning electron microscopy (FESEM, JEOL 6300-F) and high-resolution SEM (FEI Nova NanoSEM). For the transmission electron microscopy (TEM) investigation (using a JEOL 1010 operating at 100 kV and a CM20 FEG operating at 200 kV), the NWs were first ultrasonically dispersed in methanol. A drop of the suspension onto a carbon-coated copper grid was dried at room temperature and then used for TEM studies. To compare the optical properties, the NWs were studied using photoluminescence (PL) spectroscopy excited with the unfocused 325 nm line of a HeCd laser. The room-temperature PL spectra were recorded using a single monochromator connected to a liquid-nitrogen-cooled CCD camera.

Results and Discussion

Figure 1 shows schematically the NW growth furnace, highlighting the respective VS and VLS growth regions. The observation of upstream growth inside the furnace is attributed to the small dimension of the tube and the low flow rate of the Ar carrier gas, resulting in semistatic conditions, as simulated recently.[17]

Figure 2 shows (a) tilted- and (b) top-view SEM images of the as-grown VS NWs on Au patterned GaN/sapphire substrates at 930 °C. As expected, the NWs grow vertical to the substrate. The quasi-hexagonal ends of the wires (Figure 2b) indicate that their main axis is preferentially oriented along the [0001] direction, in accordance with the growth habit of wurtzite crystals. The NW diameter varies from 40 to 150 nm, which is significantly larger than the former Au dot size. Previously, we suggested a model for the interactions between the adsorbed ZnO molecules and the Au particles in the case of VS growth.[18] In brief, the Au particle surface is saturated by ZnO flakes, leading to the formation of pyramidal ZnO nuclei. These ZnO nuclei govern the NW dimensions and are responsible for the diameter deviation of the NWs. The former Au particle position controls the wire position; its size represents only the lower limit of the wire dimension.

Upon the repeated use of ILs ($BMIm^+BF_4^-$), the VS NW growth transforms into the VLS NW growth mode. In addition, the region where a successful growth is observed in our tube furnace extends drastically to ~7 cm, as depicted in Figure 1. It is noteworthy to mention here that the single use of a higher concentration of IL results in black soot that gets deposited onto the wall of the tube and is observed to hinder the NW growth. Hence, a repeated use of IL in smaller concentrations, avoiding black soot formation, is required for achieving a VLS NW growth mode. Thus, besides changing the growth mechanism from VS to VLS, the use of ILs results in an increase of the NW growth region from ~2 to ~7 cm, implying an increase in the growth yield and a growth extending into the high-

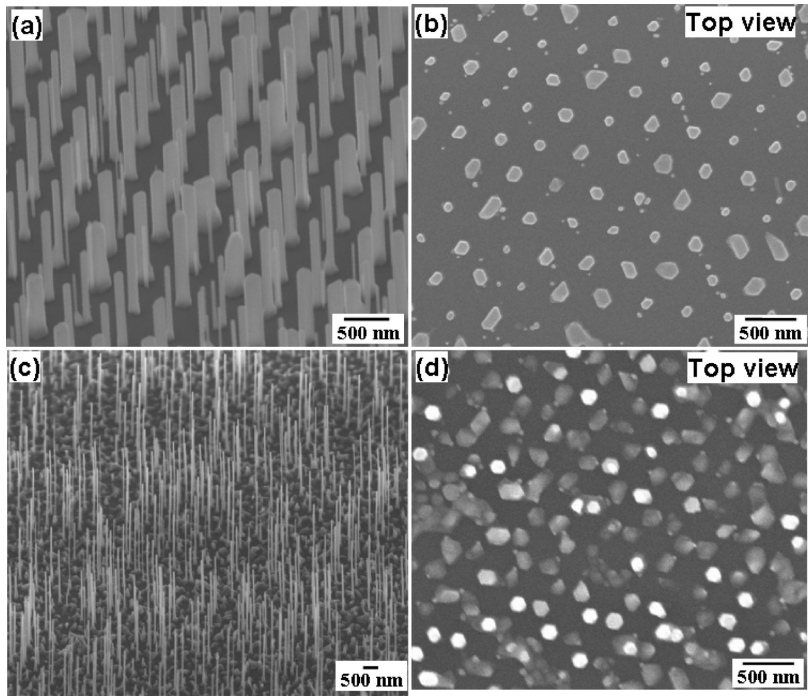

Figure 2. SEM images of VS ZnO NWs grown on Au patterned GaN/sapphire substrates: (a) 30° tilted view of the vertical NWs and (b) top view of the NWs showing their hexagonal cross section and the hexagonal pattern. SEM images of VLS ZnO NWs: (c) tilted view of NWs grown after using the IL and (d) top view of the VLS NWs.

temperature region of the furnace. The observed NWs are now characterized by the presence of Au particles at the wire tip as the typical characteristic of the VLS mechanism. Figure 2c,d shows tilted and top overview SEM images of the patterned VLS NWs grown for 30 min at 905 °C. These NWs grow vertical on the substrates and have diameters between 9 and 100 nm. However, for the successful VLS dominant (VS suppressed) growth, a significant higher O_2 flow rate of 0.1 sccm is needed along with the Ar flow rate of 7 sccm; the reason will be discussed later. In addition, not all former Au dot positions develop into a nanowire because of surface migration.

TEM investigations, as shown in Figure 3, have been carried out in order to determine the crystal structure. The VS grown NWs (Figure 3a,b) are single-crystalline with the conventional [0001] orientation (*c*-plane growth). On the other hand, the single-crystalline VLS NWs show the presence of $[2\bar{1}\bar{1}0]$ along with [0001] orientations (Figure 3d−g). The presence of Au at the wire tip, the characteristic feature of the VLS mode, is observed for all the VLS NWs (Figure 3c,h). The additionally found kinked NWs are oriented along the *a* plane $[\bar{2}11\bar{1}]$, as confirmed from SAED (Figure 3h,i).

PL can give useful information by checking the ratio of band-gap emission around 3.3 eV and defect related emission around 2.4 eV, which might be influenced by the surface quality of the wires. To avoid the contribution from the underneath GaN, the PL measurements were performed on freshly prepared samples on Si wafers under identical conditions. The VLS grown NWs show a strong and sharp UV emission at 378 nm (3.28 eV) (Figure 4) attributed to near band edge emission, arising from the recombination of free or bound excitons of ZnO.[19] The broad green emission peak around 2.4 eV (516 nm) appears for both the VS and the VLS NWs, however, with different ratios. This green emission is discussed as deep-level or trap-state emission, caused by defects of the crystal or crystal surface. The involvement of oxygen (O) vacancies, interstitial O, Zn vacancies, Zn interstitials, and other extrinsic impurities have also been discussed.[20] Surface O deficiencies are discussed as

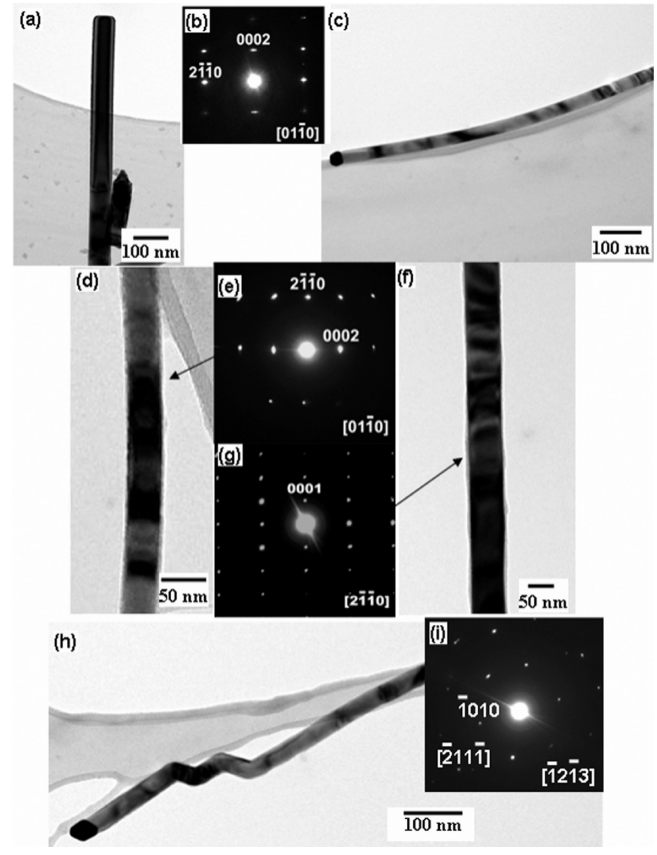

Figure 3. TEM images of VS NWs (a) and the corresponding selected area electron diffraction (SAED) (b), VLS NWs with Au dot on top (c), VLS NWs (d, f) with the corresponding SAEDs (e, g) demonstrating different orientations, VLS NWs with kink/zigzag (h) oriented along $[\bar{2}11\bar{1}]$ (i). The SAEDs confirm the single-crystalline nature of all investigated NWs.

electron capture centers, which can reduce the recombination rate of electrons and holes.[21] Very recently, we showed that

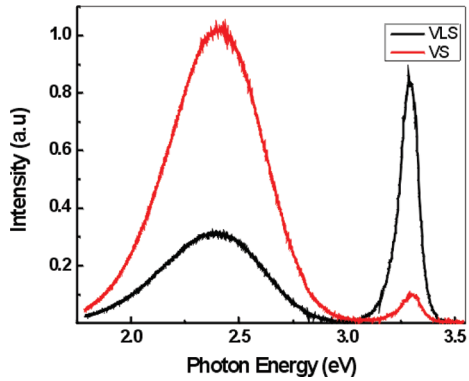

Figure 4. PL spectra recorded for as-synthesized NWs grown for 20 min on Si (100) wafers at 930 °C.

the green emission is reduced if the nanowire side walls are covered by an Al_2O_3 shell, which reduces the probability that a hole trapped at the surface tunnels into an oxygen vacancy.[22] Low-temperature measurements are under way for further clarification.

We attribute the drastic change in the growth mechanism from VS to VLS to the large number of C that is released as a result of the thermal decomposition of ILs and partly to the presence of F and N, mediating the partial polarity of the NWs. Thermogravimetric analysis of ILs implies them to be stable up to 450° and to decompose completely at above 460°. The ILs undergoes a pyrolysis into smaller hydrocarbon units, namely, ethylene, propylene, 1-butene, *trans*- and *cis*-2-butene, fluoromethane, 2-fluoropropane, 1-fluorobutane, 1-methylimidazole and 1-butylimidazole, before complete decomposition.[23] The decomposition proceeds mainly through simple thermal cleavage of the C−N bond rather than a nucleophilic attack of fluoride.

It is of significance to understand the growth mechanism and to control the morphology and the crystal quality of the resulting nanostructure. Accordingly, we performed a systematic investigation of the growth mechanism and the respective influence of various process parameters. Figure 5 schematically illustrates the steps involved in both kinds of growth processes. The carbothermal reduction takes place via the reaction

$$ZnO_{(s)} + C_{(s)} \rightarrow Zn_{(g)} + CO_{(g)} \quad (1)$$

providing the Zn source material for the NW growth. The backward reaction of eq 1 is also thermodynamically viable, but its contribution for the NW growth can be considered as negligible. In the case of VS, the growth is initiated by the formation of ZnO nuclei via an oxidation reaction

$$2Zn_{(g)} + O_{2(g)} \rightarrow 2ZnO_{(s)} \quad (2)$$

where the Au only acts as a surface inhomogeneity, serving as the preferential defect site for subsequent vapor adsorption and the O is provided externally along with the Ar carrier gas. Zn oxidation could also result from the reaction containing CO and CO_2 i.e.[24]

$$Zn_{(g)} + CO_{2(g)} + CO_{(g)} \rightarrow ZnO_{(s)} + 2CO_{(g)} \quad (3)$$

however, eq 2 is still expected to be the dominant reaction governing the growth. We reported previously that the VS growth mechanism can involve a crystallographic-direction-dependent anisotropic growth.[25] Au serves as a surface inhomogeneity or "defect" and provides the energetically favored nucleation site for the condensing vapor. The precipitation and oxidation of Zn takes place into (0001)-oriented quasi-hexagonal ZnO nuclei as also observed experimentally (Figure 6a). Finally, ZnO nucleates (bigger

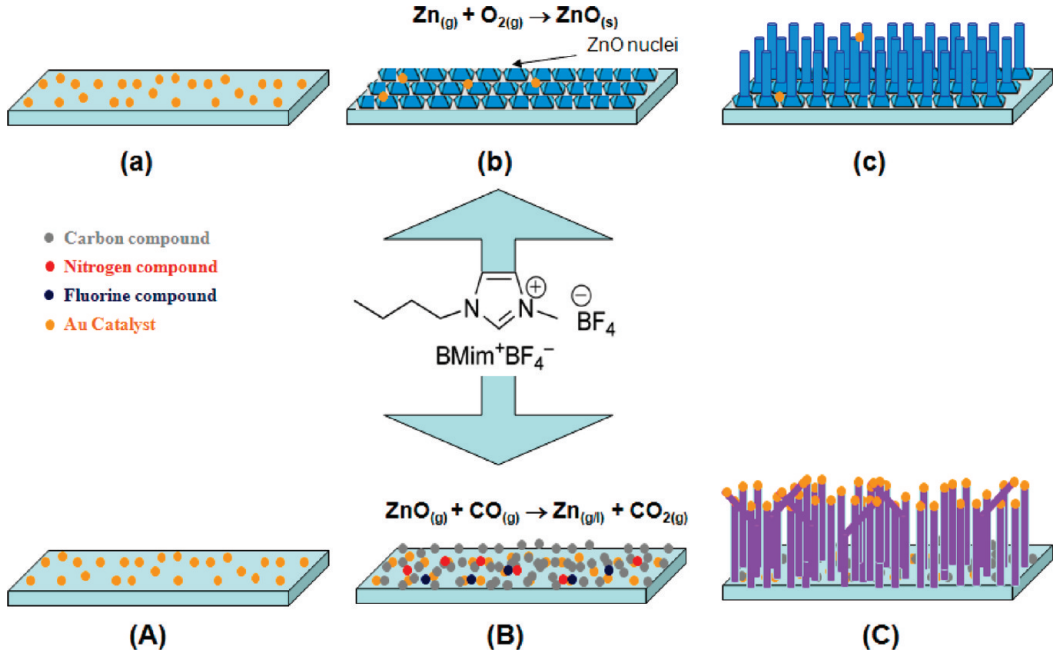

Figure 5. Steps involved in the VS (top images) and the VLS (bottom images) growth mechanisms on GaN/Si substrates. (a) Substrate with Au catalyst seeds. (b) Ramping up to higher temperatures leads to the formation of ZnO nuclei with the Au dots as favored growth sites. (c) ZnO NWs grow from these nuclei. Upon the use of the IL, the growth process transforms into a reactive VLS: (A) Au−Zn catalyst seed layer, (B) deposition of hydrogenated C (and N or F) on the substrate when the furnace is ramped at a higher temperature, and (C) NWs growing on the substrate surface with kinks and different preferred growth planes.

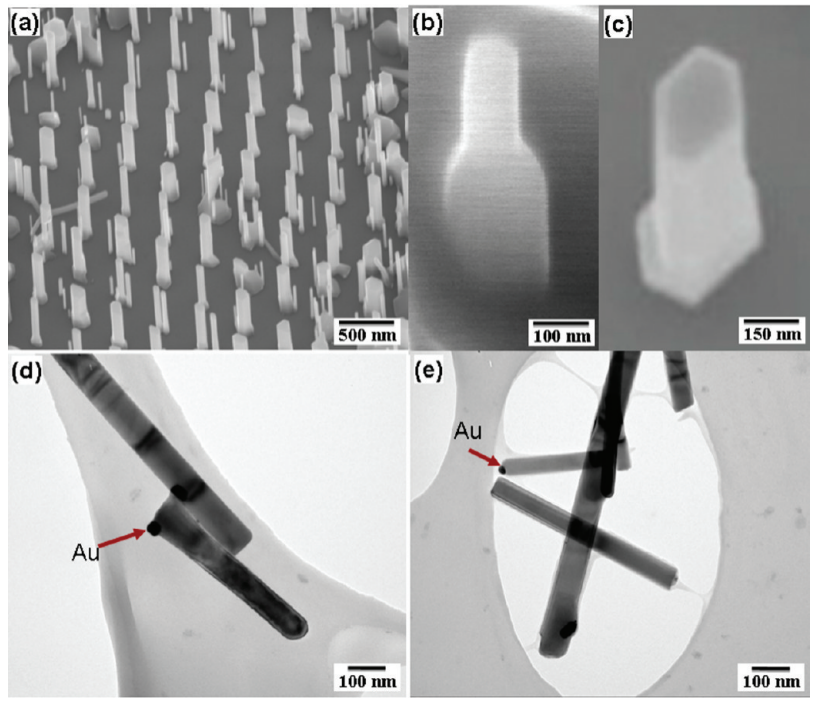

Figure 6. (a) SEM image showing the aligned quasi-hexagonal ZnO NW formation. (b, c) High-magnification images taken at a 45° and 30° tilt, respectively, showing the hexagonal pyramids underneath the NWs. TEM images showing the position of Au in the VS grown NWs mostly (d) at the base or sometimes (e) at the top of the NW.

dimension) at the top of the pyramids and grows homoepitaxially into faceted short pillars/NWs (Figure 6b,c). Au could be seen adhering mostly to the root of the NW (Figure 6d) or physically sitting on the NWs' tip (Figure 6e). The surface diffusion on solid surfaces is slow, and hence, the resulting NWs are of shorter length.

Now, in the case of VLS, the NWs grow in the region where the substrate temperature is homogeneous and almost equal to the source temperature. The decomposition of the IL results in release of (semistatic condition) hydrogenated carbon, fluorine, and nitrogen compounds (impurities) inside of the tube. Every time the furnace is ramped at high temperatures, the contaminations desorbs from the wall and adsorb on the Au-containing substrates, forming an additional source of C and O. Recently, it was demonstrated that the presence of an ultrathin carbon layer (2 nm) predeposited on the substrate surface strongly enhances the NW growth.[26] It also influences the catalyst droplets at the initial stage of VLS growth and determines the scheme of crystal growth.[10] Further, it seems to act as a buffer layer between the substrate and the catalyst nuclei, enhancing the NWs' growth.[27] A simple patterning of the wafer with photoresists/hydrogenated amorphous C has also been demonstrated to control the region of growth.[28] We note here that the experiments carried out with the patterned Au using photoresist techniques (without plasma treatment and annealing) also exhibited a VLS type of growth mechanism, further supporting the role of C.

Of the various gases, in particular, CO is known to adsorb strongly on quartz and could even result in the formation of Zn following equation

$$ZnO_{(s)} + CO_{(g)} \rightarrow Zn_{(g/l)} + CO_{2(g)} \quad (4)$$

For conditions similar to VS, reaction 4 implies that, at initial stages, most of the ZnO formed via reaction 2 might be converted back to Zn on the substrate containing Au, thereby increasing the Zn concentration. The metallic Zn subsequently forms a liquid alloy with the Au present on the substrate, and at the deposition temperatures used here (below the boiling point of Zn and well in the eutectic range of the Zn−Au system), these alloy droplets are highly mobile on the substrate surface (Figure 7a) and, hence, result in the formation of a film (Figure 7b) and a subsequent pattern collapses (Figure 7c). Please note that, for the temperature available in the VLS region (875−930 °C), already the inclusion of 15 atom % of Zn into the Au is enough to result in a melted Au−Zn droplet.[29] If the droplet gets more and more Zn and no other process takes place, the size of the dot gets bigger. On a certain point, a segregation of liquid Zn might take place and a crawling of the droplet on the surface takes place, leaving a track of Zn behind, as can be seen in Figure 7a and partly also in Figure 7b. If now oxygen is available, then that out-sourced liquid Zn oxidizes, forming solid ZnO and hence starting the ZnO wire. The still liquid Au−Zn alloy at the top governs the efficient adsorption of the Zn gas. It is also interesting to note here that some of the wires in VS dominant condition do exhibit a sidewise crawling of NWs, starting from the root (Figure 6a). This is probably due to the contribution arising from eq 4. The difference in the VS and the VLS processes involving the liquid Au−Zn phase is the amount of Zn segregating-out and the O available to oxidize that Zn immediately. The whole process is actually controlled by the carbon species in the furnace controlling the amount of Zn gas, by the flow conditions and by the availability of oxygen. By following this route, consequently, the process should be called a *reactive VLS mode*. The solid ZnO phase is based on the Zn reaction with a reliable O source. ZnO is not soluble in Au; the ZnO and Au phases exist independently from each other.

Here, it is also significant to know that the choice of process parameter can effectively switch a growth mechanism from VLS to VS. Importantly, by optimizing the O_2 inside the system, it is possible to switch the equilibrium toward either reaction 4 or reaction 2. For example, Figure 2c depicts the patterned

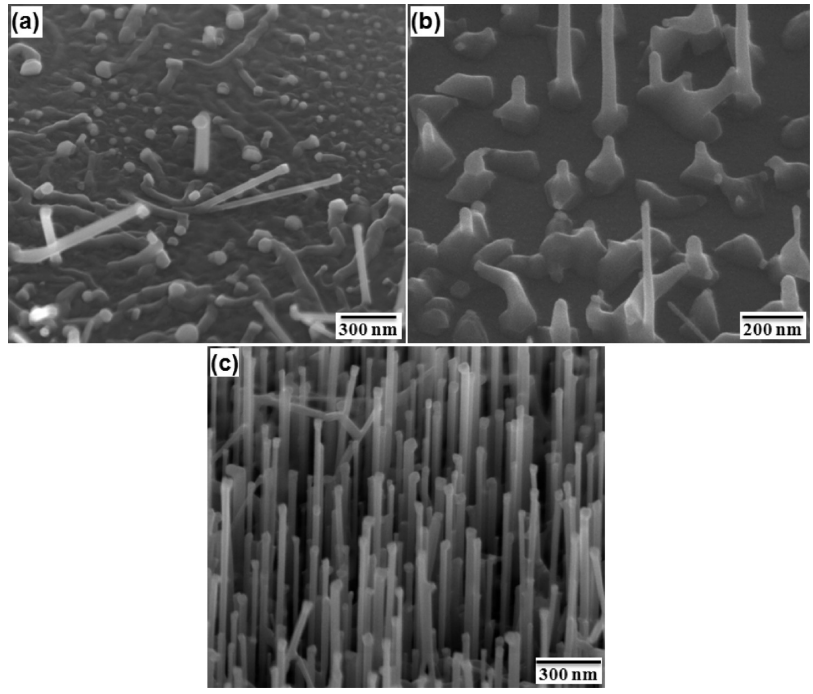

Figure 7. SEM images of samples grown on the GaN/sapphire substrate at 930 °C, showing (a) surface crawling of liquid Au−Zn alloy droplets at the substrate surface, destroying the patterning, (b) starting growth of oxidized nuclei, and (c) resulting NWs after the initial pattern collapsed.

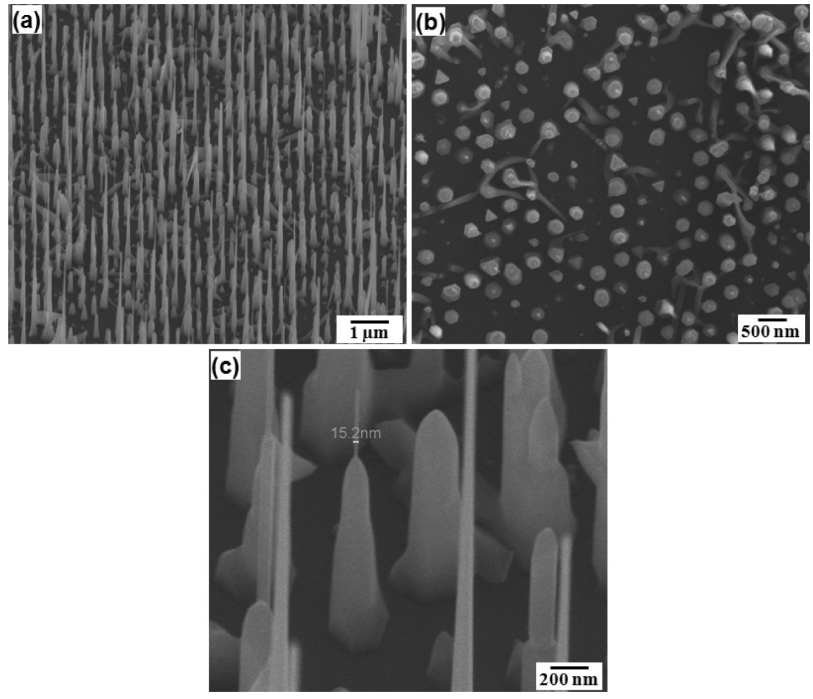

Figure 8. (a) SEM image (at a 45° tilt) of NWs grown at 930 °C for 20 min with a high O_2 flow rate of 2 sccm. (b) Top view showing the hexagonal pattern in accordance with the template. (c) Magnified image of tapered NWs showing small NWs growing at its apex with a diameter of ∼15 nm, as per the VLS mechanism.

growth of VLS NWs, which is possible with an increased flow rate of O_2 (0.1 sccm), where the additional O_2 helps to sustain the ZnO formation, thereby restricting the surface migration. In other words, higher O_2 increases the rate of Zn oxidation, as per reaction 2, in comparison with ZnO reduction, as per reaction 4. Also, this fast oxidation suppresses the liquid Au−Zn alloy formation and hence not all Au dots result in NWs. This further implies that, at temperatures above the boiling point of Zn (907 °C) and with a high O_2 flow rate, it should be possible to suppress the VLS mode completely and reverse the growth mechanism back to the VS mode (ZnO melting point = 1975 °C). Interestingly, for a substrate temperature of 930 °C (avoiding liquid-state formation) and a high O_2 flow rate of 2 sccm, we again observed VS NWs, as demonstrated in Figure 8. As expected, these NWs have bigger dimensions (between 80 and 300 nm) with small diameter NWs (VLS) growing on top of bigger ones (Figure 8c). These smaller NWs are anticipated to grow during cooling the system when the temperature approaches the boiling point of Zn. VS NWs at such a higher deposition temperature are otherwise impossible

for the pure system; however, reaction 4, as a result of the IL and the semistatic system, enabled respective conditions for the growth of such NWs. The VS state of the growth tube is easily recovered by cleaning with concentrated hydrochloric acid (HCl), thereby implying the complete reversible switching between VS and VLS NW growth modes. HCl is known to degrade ZnO and is used as a common cleaning agent for the quartz tube used for the NW growth. HCl is also highly reactive toward organic molecules and carbonates. Further, firing at a higher temperature of ~1000 °C assures complete cleaning of the tube. Removal of contamination implies the growth to be VS-driven.

Thus, the presence of the additional C (to reduce the ZnO to Zn) from the IL and a reliable O source (to react with the outsourced Zn at the alloy droplet) are responsible for switching the growth mechanism from VS to VLS. The presence of liquid Zn is crucial for the VLS mechanism, which can interact with the Au present on the substrate, resulting in Au−Zn alloy droplets that govern the NWs' growth. This is otherwise not possible in the pristine clean system where the Zn oxidation is the only dominant reaction. Further, we believe that CO might get adsorbed uniformly on the whole substrate at the used deposition temperatures and is hence responsible for the increased growth region and yield. Consequently, reactions 2 and 4 coupled with the other process parameters, namely, temperature and O_2 flow rate, can effectively be used to suppress or enhance the VLS mechanism. Similar results of transformation from VS to reactive VLS were observed for another IL, namely, butyl methyl imadazolium hexafluorophosphate ($BMIm^+PF_6^-$), which we used to repeat the process and which confirmed the generality of the process.

In summary, a reversible switching between the VS to the reactive VLS growth mechanism has been demonstrated for the first time by adding or removing an ionic liquid and by a careful control of process parameters. Formation of liquid Zn and a subsequent liquid Au−Zn alloy due to an additional carbon source in the system are mandatory for the VLS transition. Our results clarify, for the first time, the reason for the different roles of Au, that is, acting as surface defects or as a catalyst in VS and VLS growth modes, respectively. Reactions 2 and 4 along with the process parameters, namely, temperature and O_2 flow rate, can effectively be used to suppress or enhance the VLS mechanism. Further, the NW growth region increases drastically from ~2 to ~7 cm from VS to VLS under similar experimental conditions. Complete reversibility to the VS mechanism is achieved by cleaning the tube with concentrated HCl. Thus, our results demonstrate the possibility of controlling not only the growth mode and region but also the crystal quality of the NWs by using ILs as an additional carbon source. The present work is a crucial step toward a better understanding and realizing designed NWs based on VS or VLS for a particular application.

Acknowledgment. N.S.R. would like to acknowledge the Alexander von Humboldt Foundation for the fellowship. K.S. and M.Z. acknowledge the support from DFG ZA 191/17. We are also thankful to Dr. E. Redel for providing the ionic liquid, S. Gutsch for help with the HRSEM investigations, and D. Hiller for the PL measurements.

References and Notes

(1) Subannajui, K.; Kim, D. S.; Zacharias, M. *J. Appl. Phys.* **2008**, *104*, 014308.
(2) Hong, W.-K.; Sohn, J. I.; Hwang, D.-K.; Kwon, S.-S.; Jo, G.; Song, S.; Kim, S.-M.; Ko, H.-J.; Park, S.-J.; Welland, M. E.; Lee, T. *Nano Lett.* **2008**, *8*, 950.
(3) Goldberger, J.; Sirbuly, D. J.; Law, M.; Yang, P. *J. Phys. Chem. B* **2005**, *109*, 9.
(4) Könenkamp, R.; Word, R. C.; Schlegel, C. *Appl. Phys. Lett.* **2004**, *85*, 6004.
(5) Law, M.; Greene, L. E.; Johnson, J. C.; Saykally, R.; Yang, P. D. *Nat. Mater.* **2005**, *4*, 455.
(6) Yang, P.; Yan, H.; Mao, S.; Russo, R.; Johnson, J.; Saykally, R.; Morris, N.; Pham, J.; He, R.; Choi, H.-J. *Adv. Funct. Mater.* **2002**, *12*, 323.
(7) Fan, H. J.; Werner, P.; Zacharias, M. *Small* **2006**, *2*, 700.
(8) Hughes, W. L.; Wang, Z. L. *J. Am. Chem. Soc.* **2004**, *126*, 6703.
(9) Kar, S.; Pal, B. N.; Chaudhuri, S.; Chakravorty, D. *J. Phys. Chem. B* **2006**, *110*, 4605.
(10) Wang, Z. L. *ACS Nano* **2008**, *2*, 1987.
(11) Wagner, R. S.; Ellis, W. C. *Appl. Phys. Lett.* **1964**, *4*, 89.
(12) Zhu, Z.; Chen, T.-L.; Gu, Y.; Warren, J.; Osgood, R. M. *Chem. Mater.* **2005**, *17*, 4227.
(13) Dai, Z. R.; Pan, Z. W.; Wang, Z. L. *Adv. Funct. Mater.* **2003**, *13*, 9.
(14) Ho, S.-T.; Wang, C.-Y.; Liu, H.-L.; Lin., H.-N. *Chem. Phys. Lett.* **2008**, *463*, 141.
(15) Morris, R. J. H.; Dowsett, M. G.; Dalal, S. H.; Baptista, D. L.; Teo, K. B. K.; Milne, W. I. *Surf. Interface Anal.* **2007**, *39*, 898.
(16) Fan, H. J.; Bertram, R.; Dadgar, A.; Christen, J.; Krost, A.; Zacharias, M. *Nanotechnology* **2004**, *15*, 1401.
(17) Subannajui, K.; Ramgir, N.; Grimm, R.; Michiels, R.; Yang, Y.; Müller, S.; Zacharias, M. *Cryst. Growth Des.* **2010**, *10*, 1585.
(18) Kim, D. S.; Scholz, R.; Gosele, U.; Zacharias, M. *Small* **2008**, *4*, 1615.
(19) Bae, S. Y.; Seo, H. W.; Park, J. *J. Phys. Chem. B* **2004**, *108*, 5206.
(20) Zhang, Y.; Lu, F.; Wang, Z.; Zhang, L. *J. Phys. Chem. C* **2007**, *111*, 4519.
(21) Kuo, T.-J.; Lin, C.-N.; Kuo, C.-L.; Huang, M. H. *Chem. Mater.* **2007**, *19*, 5143.
(22) Richters, J.-P.; Voss, T.; Kim, D. S.; Scholz, R.; Zacharias, M. *Nanotechnology* **2008**, *19*, 305202.
(23) Ohtani, H.; Ishimura, S.; Kumai, M. *Anal. Sci.* **2008**, *24*, 1335.
(24) Osborne, J. M.; Rankin, W. J.; Mccarthy, D. J.; Swinbourne, D. R. *Metall. Mater. Trans. B* **2001**, *32B*, 37.
(25) Fan, H. J.; Lee, W.; Hauschild, R.; Alexe, M.; Rhun, G. L.; Scholz, R.; Dadgar, A.; Nielsch, K.; Kalt, H.; Krost, A.; Zacharias, M.; Gösele, U. *Small* **2006**, *2*, 561.
(26) Yanagida, T.; Marcu, A.; Matsui, H.; Nagashima, K.; Oka, K.; Yokota, K.; Taniguchi, M.; Kawai, T. *J. Phys. Chem. C* **2008**, *112*, 18923.
(27) Banerjee, D.; Jo, S. H.; Rem, Z. F. *Adv. Mater.* **2002**, *22*, 2028.
(28) Cheng, C.; Lei, M.; Feng, L.; Wong, T. L.; Ho, K. M.; Fung, K. K.; Loy, M. M. T.; Yu, D.; Wang, N. *ACS Nano* **2009**, *3*, 53.
(29) Okamoto, H.; Massalski, B. T. *Bull. Alloy Phase Diagrams* **1989**, *10*, 59.

JP909377B